CO_2 Foaming of Poly(ethylene glycol)/Polystyrene Blends: Relationship of the Blend Morphology, CO_2 Mass Transfer, and Cellular Structure

Kentaro Taki, Kouei Nitta, Shin-Ichi Kihara, Masahiro Ohshima

Department of Chemical Engineering, Kyoto University, Kyoto 615-8510, Japan

Received 10 May 2004; accepted 21 December 2004
DOI 10.1002/app.21930
Published online in Wiley InterScience (www.interscience.wiley.com).

ABSTRACT: When polymer blends are foamed by physical foaming agents, such as CO_2 or N_2, not only the morphology and viscosity of the blend polymers but also the solubility and diffusivity of the physical foaming agents in the polymers determine the cellular structure: closed cell or open cell and monomodal or bimodal. The foam of poly(ethylene glycol) (PEG)/polystyrene (PS) blends shows a unique bimodal (large and small) cellular structure, in which the large-size cells embrace a PEG particle. Depending on the foaming condition, the average size of the large cells ranges from 40 to 500 μm, whereas that of small cells becomes less than 20 μm, which is smaller than that of neat PS foams. The formation mechanism of the cellular structure has been investigated from the viewpoint of the morphology and viscosity of the blend polymer and the mass-transfer rate of the physical foaming agent in each polymer phase. The solubility and diffusivity of CO_2, which determine the mass-transfer rate of CO_2 from the matrix to the bubbles, were measured by a gravimetric measurement, that is, a magnetic suspension balance. The solubility and diffusivity of CO_2 in PS differed from those in PEG: the diffusion coefficient of CO_2 in PEG at 110°C was 3.36×10^{-9} m^2/s, and that in PS was 2.38×10^{-10} m^2/s. Henry's constant in PEG was 5600 cm^3 (STP)/(kg MPa) at 110°C, and that in PS was 3100 cm^3 (STP)/(kg MPa). These differences in the transport properties, morphology of the blend, and CO_2-induced viscosity depression are the control factors for creating the unique cellular structure in PEG/PS blends. © 2005 Wiley Periodicals, Inc. J Appl Polym Sci 97: 1899–1906, 2005

Key words: blends; diffusion; foams

INTRODUCTION

Polymers are often blended to create new functions, which each polymer alone cannot express, or to compensate for the weakness in the mechanical properties of each polymer. In polymeric foaming also, polymer blends are often used to create fine cell structures.[1–3]

Recently, environmental concern has led the plastic foaming industries to investigate a technology with environmentally benign foaming agents, such as CO_2 and N_2. Therefore, research on the foaming of blend polymers with CO_2 has become important.

Foaming occurs by the dissolution of CO_2 into a molten polymer under high pressure and then the release of the pressure or an increase in the temperature to liberate the dissolved CO_2. Doroudiani et al.[4] studied the foaming of high-density polyethylene (HDPE)/isotactic polypropylene (PP) blends. They found that a fine cellular structure could be created in the blend polymer by choosing a suitable temperature, whereas little or no foaming took place in each neat polymer. Rachtanapun et al.[5] studied the foaming of HDPE/PP blends and reported that the foaming ratio was increased by blending. Lee et al.[6] foamed 80/20 low-density polyethylene (LDPE)/polystyrene (PS) blends with CO_2 by an extruder and mentioned that the resulting cellular structure of the LDPE/PS blends was not changed from that of the pure polymers. Siripurapu et al.[7] investigated PS/poly(vinylidene fluoride) (PVDF) and poly(methyl methacrylate) (PMMA)/PVDF blends for foaming to expand the operating windows and concluded that blending PS with PVDF was not suitable for foaming because of immiscibility, whereas PMMA/PVDF could be foamed at various operating conditions. In those studies, the intent of the blending was to expand the operating window of foaming conditions and to create a uniform and fine cellular structure. Krause et al.[8] studied a polysulfone/polyimide blend to make an open cell structure by foaming with CO_2. They successfully created the open cell structure; however, they could not obtain clear insight into the formation mechanism of the open cell structure in the blends.

When polymer blends are foamed, the cellular structure is determined not only by the morphology and viscosity of the blend polymers but also by the solubility and diffusivity of the physical foaming agent in the polymers. Therefore, there is a strong

Correspondence to: M. Ohshima.

TABLE I
Weight Fractions of the Blend Samples

	PS100	PEG10/PS90	PEG25/PS75	PEG40/PS60
PEG	0	10	25	40
PS	100	90	75	60

possibility of creating various cell structures by the blending of polymers. In this study, poly(ethylene glycol) (PEG)/PS blends were foamed by CO_2. The foam of the PEG/PS blends showed a unique bimodal cellular structure, in which PEG particles were embraced in larger cells, whereas the average size of the smaller cells became smaller than that created by the foaming of PS alone at the same temperature and pressure conditions. The mechanism of foaming such a unique cellular structure of PEG/PS was investigated from the viewpoint of the transport properties of CO_2 and the viscosity and morphology of the blend.

EXPERIMENTAL

Materials

PS with a weight-average molecular weight of 3.21×10^5 was obtained from Idemitsu Petrochemical Co., Ltd. (Chiba, Japan). PEG with a weight-average molecular weight of 4×10^6 was purchased from Wako Pure Chemical Industries, Ltd. (Osaka, Japan). A twin-screw extruder (TSE16mm, Prism, Staffordshire, UK) was used to blend PEG with PS at different weight fractions at the screw rotating speed of 300 rpm. The weight fractions of the blends and their abbreviations are listed in Table I. CO_2 (Kyoto Teisan, Kyoto, Japan; 99.9% pure) was used as a physical foaming agent.

The glass-transition temperature or melting temperature of each sample was measured with a differential scanning calorimeter (Pyris 1, PerkinElmer, Wellesley, MA) at the rate of 10°C/min above room temperature. The resulting melting and glass-transition temperatures of the neat polymer samples are listed in Table II.

Measurements of the solubility and diffusivity

Physical polymeric foaming can be divided into four processes: (1) the dissolution of the physical foaming agent into the polymer, (2) bubble nucleation in the polymer, (3) bubble growth, and (4) bubble coalescence and stabilization. The mass-transfer properties of the foaming agent in the polymer, that is, the solubility and the diffusivity of CO_2 in the polymer, are the key parameters in all four processes and determine the final cell structure. We used a magnetic suspension balance (MSB; Rubotherm and Bel Japan, Osaka, Japan) to measure the solubility and diffusivity of CO_2 in the polymer. When CO_2 dissolves in the polymer, the weight of the polymer increases because of the weight of dissolved CO_2. Thus, weighing the polymer in pressurized CO_2 allows us to determine the solubility and diffusion coefficient of CO_2. The MSB makes it possible to weigh samples under high-pressure and temperature environments without the balance being held in the environments. The measurement scheme is detailed elsewhere.[9] When CO_2 dissolves in the polymer, it swells the polymer. Because the buoyancy caused by the swelling affects the solubility measurements, the specific volume of the polymer/CO_2 mixture should be estimated accurately to obtain the true transport properties. The specific volume at a given temperature and a pressure can be calculated with the Sanchez–Lacombe equation of state (S–L EOS) and a mixing rule with a binary interaction parameter.[10,11] The characteristic parameters of S–L EOS of each polymer were determined from pressure–volume–temperature data and/or the literature.[9,12] The resulting parameter values are listed in Table III. The solubility and the diffusivity of CO_2 in PEG and PS were measured at 110°C and in a pressure range of 4–15 MPa.

Rheometry

To measure the storage and loss moduli of both PEG and PS, a temperature scan of a dynamic frequency sweep test with a tensing fixture was carried out with a Rheogel-E4000 (UBM, Kyoto, Japan). The frequency was set at 10 Hz for all measurements. The temperature was changed from 50 to 150°C at the rate of 3°C/min.

Foaming

Batch physical foaming

The following procedure was used to foam the blend polymers in a high-pressure vessel. Disk-shaped samples, 20 mm in diameter and 3 mm thick, were made by the polymer blends being kept in a hot press at 200°C and 10 MPa for 5 min. Then, a sample was placed in the high-pressure vessel. The vessel was heated to the desired foaming temperature, 110°C, which was above the melting temperature of the semicrystalline polymer, PEG. Then, the vessel was pressurized by CO_2 up to 10 MPa. After equilibrium was established, the pressure in the vessel was quickly

TABLE II
Melting Temperature (T_m) and Glass-Transition Temperature

Material	T_m (°C)	T_g (°C)
PS	—	104
PEG	68	—

TABLE III
Characteristic Parameters of S–L EoS

	Temperature T* (K)	Pressure P* (MPa)	Density ρ^* (kg/m^3)	Interaction Parameter k_{12}	Reference
PS	697.6	344.1	1093	0.1377	—
PEG	646.0	506.0	1189	0.0513	12
CO_2	341.2	369.1	1253		9

released (at a rate of ca. 5 MPa/s) to nucleate bubbles in the polymer.

After the samples were dried at 50°C *in vacuo* for 24 h, the cell structure of the resulting foamed sample was observed with a scanning electron microscope (Tiny-SEM, Technex Lab Co., Ltd., Tokyo, Japan) at an acceleration voltage of 15 kV. The cut section was coated with Au–Pd before microscopy observations. To determine the effect of the morphology of the polymer blends on the cell structure, the morphology of a nonfoamed sample was also observed with scanning electron microscopy (SEM).

Visual observation of batch physical foaming

To observe bubble nucleation and growth rates in each polymer phase *in situ*, visual observation experiments were performed. The details of the experimental setup have been given elsewhere.[13,14] To observe the differences in these rates at each polymer phase, PEG and PS samples were foamed under the same conditions. That is, a rectangular piece 10 mm long, 5 mm wide, and 0.6 mm thick was made from each polymer, and these were welded into one piece by the hot press at 200°C and 10 MPa. The sample piece was placed on the visual observation apparatus, and then it was foamed at 110°C by the release of CO_2 pressure from 10 to 0.1 MPa at a rate of 0.5 MPa/s. The bubble nucleation and growth behaviors were observed in the PS and PEG phases simultaneously.

RESULTS AND DISCUSSION

Solubility and diffusivity of CO_2 in PEG and PS

Figure 1 shows the solubility of CO_2 in PEG and PS. It was measured at 110°C from 5 to 15 MPa. The solubility of CO_2 in PEG was 1.8 times as large as that in PS at 10 MPa. Henry's constants of PS and PEG were 3100 and 5600 cm^3 (STP)/(kg MPa), respectively.

Figure 2 shows the diffusion coefficient of CO_2 in PEG and PS at 110°C. Each diffusion coefficient was measured with stepwise pressure increases of 1.0 MPa from a saturated state. The mutual diffusion coefficient was then determined by the measurement of the time evolution of the weight of the molten polymer in the course of reaching a new steady state from an old one. For example, the diffusion coefficient at 5 MPa was determined from the time evolution data of the sample weight obtained by a change in the MSB chamber pressure from 4 to 5 MPa. The average diffusion coefficients, illustrated by solid lines, were 3.36×10^{-9} m^2/s for PS and 2.38×10^{-10} m^2/s for PEG. The diffusion coefficient of CO_2 in PEG was 14.1 times as fast as that in PS.

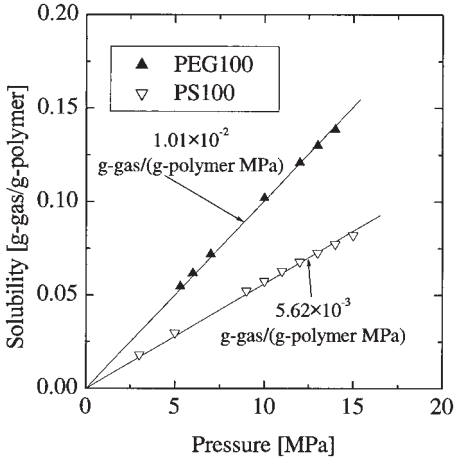

Figure 1 Solubility of CO_2 in PEG and PS at 110°C and pressures ranging from 5 to 15 MPa.

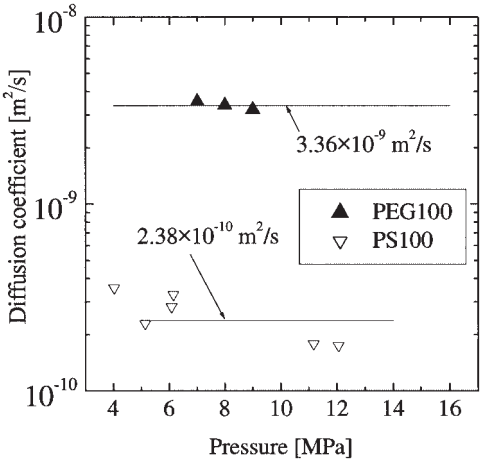

Figure 2 Diffusion coefficient of CO_2 in PEG/PS at 110°C and at pressures ranging from 5 to 12 MPa.

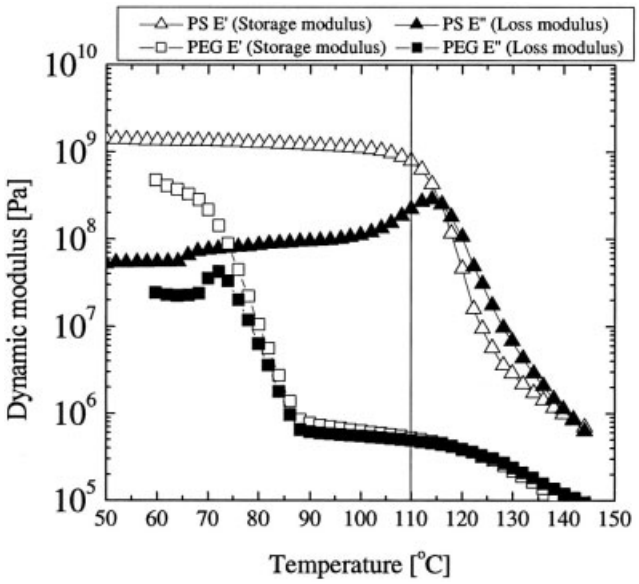

Figure 3 Storage and loss moduli of neat PEG and PS by tensing fixtures.

Rheological properties

The analysis of storage and loss moduli is useful in ascertaining the performance of a sample under stress and temperature conditions. Figure 3 shows the storage and loss moduli of PEG and PS. Both the storage and loss moduli of PEG decreased sharply above the melting temperature, and those of PS decreased above the glass-transition temperature. At the foaming temperature, 110°C, those of PS were larger than those of PEG, and the differences between PEG and PS were quite large.

Foaming

Batch physical foaming

Figure 4 shows the SEM micrographs of nonfoamed PEG/PS blends and foamed PEG/PS blends. The micrographs in the left column show the morphology of the PEG/PS blends before foaming. The micrographs in the middle column show the cell structure of the foamed blends, and those of the right column are enlarged pictures of the middle column.

Because PEG and PS are immiscible with each other, the island–sea morphology was established at these weight fractions: PEG particles became islands, and PS made the matrix. Some PEG particles were lost when the samples were prepared for SEM observations, and this resulted in voids in the matrix. As can be seen in the picture in the left column, an increase in the PEG weight fraction made the number of the island increase.

Figure 5 shows an enlarged SEM micrograph of the PEG10/PS90 blend foamed at 110°C and 10 MPa. It clearly shows a bimodal cell size structure, in which

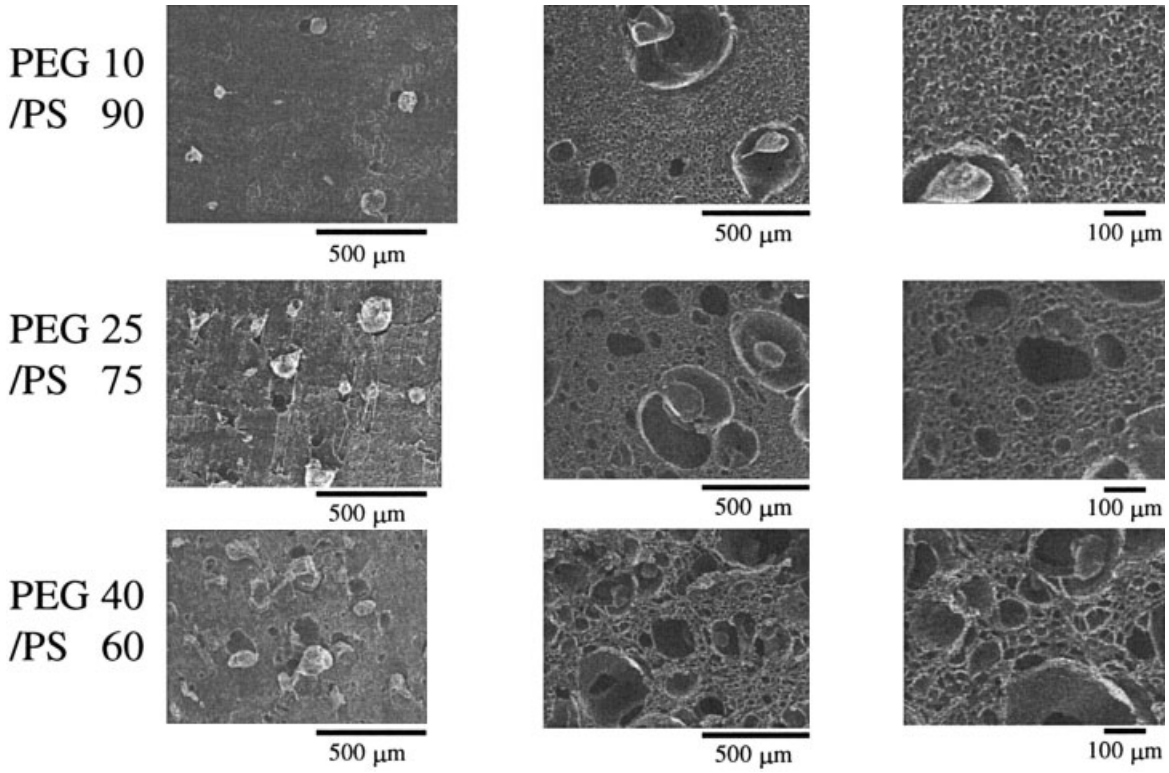

Figure 4 Micrographs of foamed and nonfoamed blends: PEG10/PS90, PEG25/PS75, and PEG40/PS60.

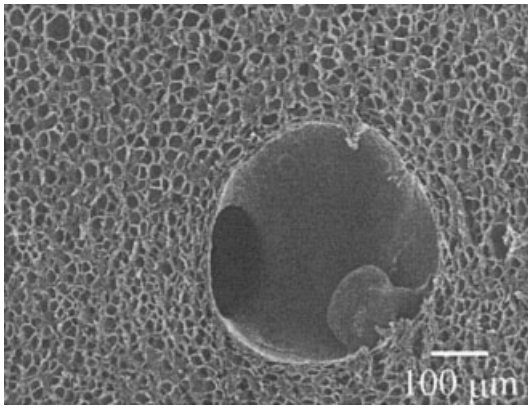

Figure 5 Cellular structure of the PEG10/PS90 blend foam prepared at 110°C and 10 MPa.

the average diameter of the smaller cell was less than 30 μm and the size of the larger cell was about 400 μm. A PEG particle was located at a large cell in the foams. Counting the cells whose diameters were larger than 40 μm at the six different positions in each micrograph and averaging the counted numbers gave the average number of large cells. The number density of large cells (N_f) was then calculated as follows:[15]

$$N_f = (nM^2/A)^{3/2} \quad (1)$$

where n is the number of cells in the micrograph, M is the magnification, and A is the actual area of the micrograph.

Figure 6 shows the relationship between the number density of large cells and the weight fraction of PEG in the blend. As the fraction of PEG increased, the number of large cells increased. This indicated that the

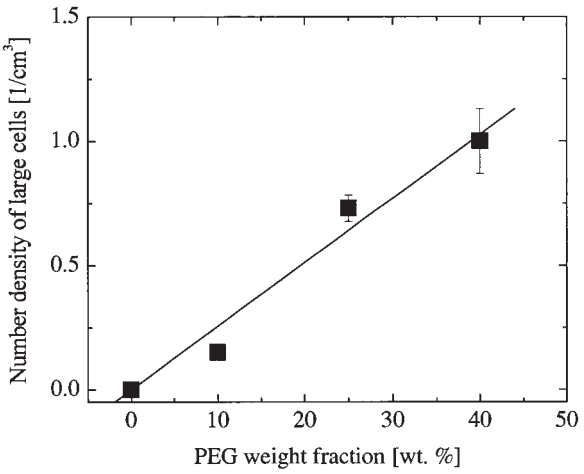

Figure 6 Relationship between the PEG weight fraction and number density of large cells in PEG/PS blends foamed at 10 MPa and 110°C.

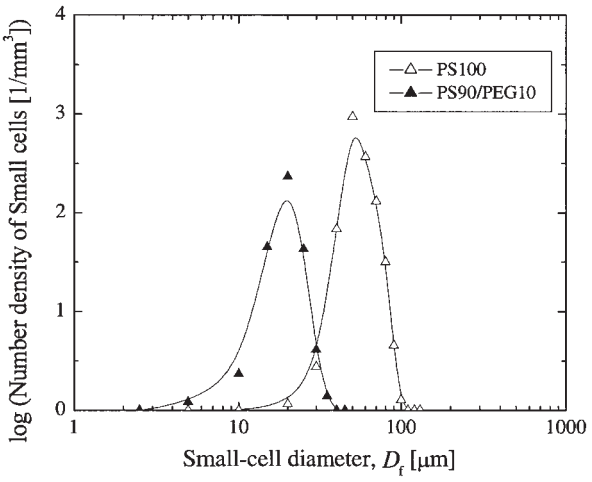

Figure 7 Size distributions of cells of PS foam and small cells in PEG10/PS90 foam.

large cells originated in the PEG phase and the small cells originated in the PS phase of the blend.

As can be seen in the micrographs of the PEG10/PS90 foam, there existed many smaller cells around larger cells. The diameter of the smaller cells was calculated from the cross-sectional area of the cells, under the assumption that a cell took a spherical shape. The cell size distribution of the PEG10/PS90 foam is illustrated in Figure 7 together with that of a neat PS foam for reference. As illustrated in Figure 7, the size of smaller cells in the foamed PEG10/PS90 blend became smaller than that of neat PS foamed under the same conditions. Blending PEG with PS created numerous large cells originating in the PEG islands, and at the same time, it reduced the size of the cells nucleating at the PS matrix. Taking the cell size at the peak of the distribution as the average cell size of small cells in the blend foam, we analyzed the effects of the PEG fraction on the size and density of the small cells. Figure 8 shows how the cell diameter and density of the small cells in the blend foam were changed by the weight fraction of PEG. As the PEG fraction increased up to 25%, the cell size decreased, and the number density increased. Then, when the fraction went over 25%, the cell size increased, and the number density decreased.

Visual observation of batch physical foaming

Figure 9 shows a series of micrographs obtained by visual observation experiments of PEG/PS foaming. The left-hand side of the micrograph is the PEG phase, and the right is the PS phase. The black dots are bubbles. In Figure 9, an arrow indicates the interface between the PEG and PS phases. After CO_2 pressure was released, numerous bubbles were nucleated and grown in the PEG phase. Slightly after the foaming of

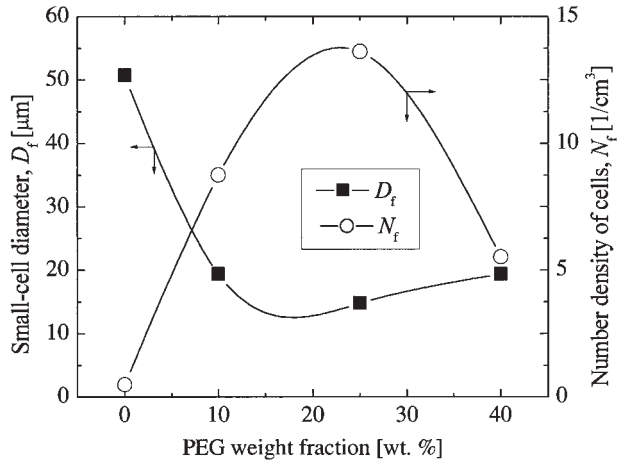

Figure 8 Effect of the PEG weight fractions on the average diameter and number density of small cells.

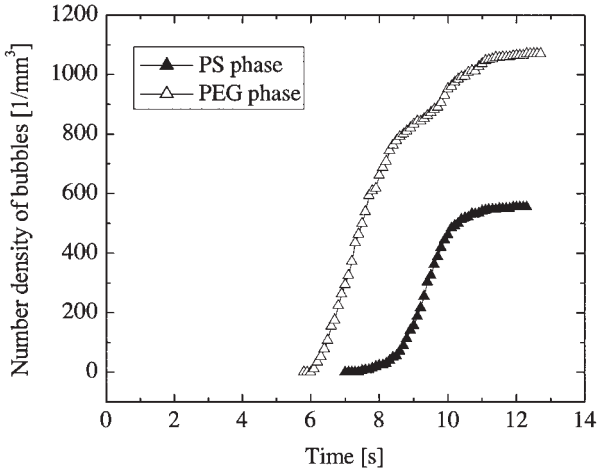

Figure 10 Number density of bubbles in PEG/PS foamed at 110°C and 10 MPa.

the PEG phase, nucleation and bubble growth occurred in the PS phase. The interface between the PEG and PS phase moved toward the PS phase because of the time difference of the foaming at the two phases. The bubbles in the PEG phase coalesced easily.

The bubble nucleation and bubble growth rates at each phase were analyzed quantitatively with image processing. Figure 10 shows the change in the cumulative number of bubbles against the time elapsed from the pressure release. Figure 11 shows the bubble growth rates in the PEG and PS phases. Each plot represents an average growth rate of the bubbles born at the time, that is, the rate of change in the cross-sectional area of bubbles that were newly observed at the time indicated.

As shown in Figure 10, bubbles started nucleating at 6 s in PEG and at 7 s in PS. The number density of nucleating bubbles in the PEG phase was larger than that in the PS phase. The bubble nucleation was enhanced in the PEG phase because the solubility of CO_2 in PEG was larger than that in the PS phase, as illustrated in Figure 1.

As shown in Figure 11, the bubble growth rate in the PEG phase was faster than that in the PS phase. Our previous study on batch foaming experiments found that bubble growth was a mass-transfer-controlled process.[14] In other words, the mass-transfer rate of CO_2 from the polymer to a bubble determines the

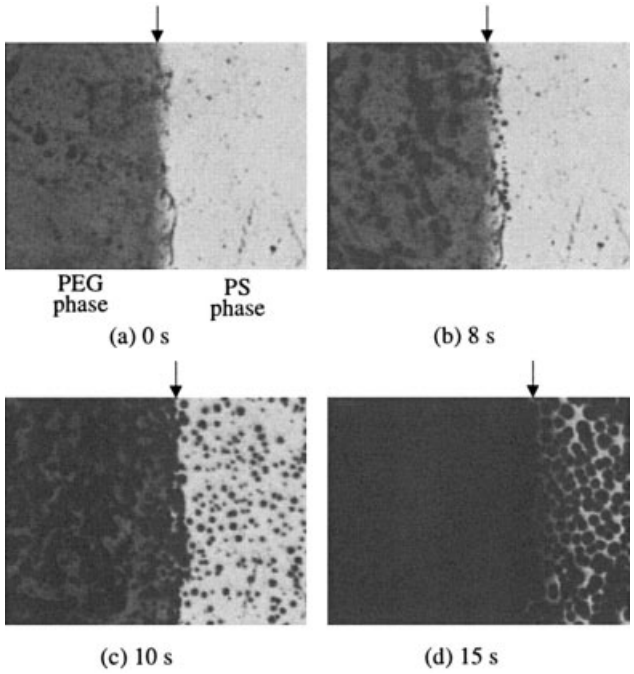

Figure 9 Series of micrographs obtained from the visual observation experiments of PEG/PS foaming. The micrographs were taken at (a) 0, (b) 8, (c) 10, and (d) 15 s. The size of the view is 1.2 mm × 1.6 mm.

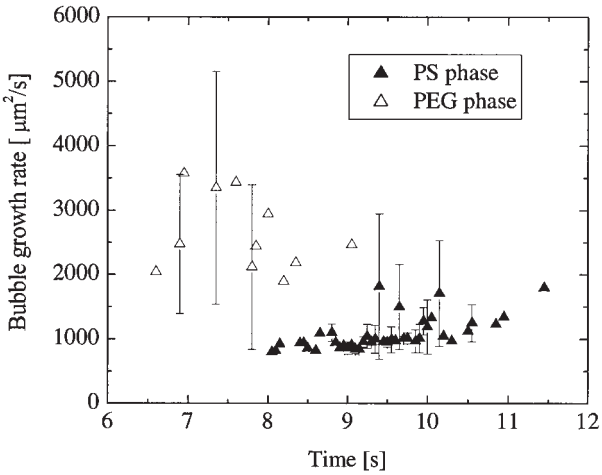

Figure 11 Bubble growth rates in the PEG phase and in the PS phase of the blend foamed at 110°C and 10 MPa.

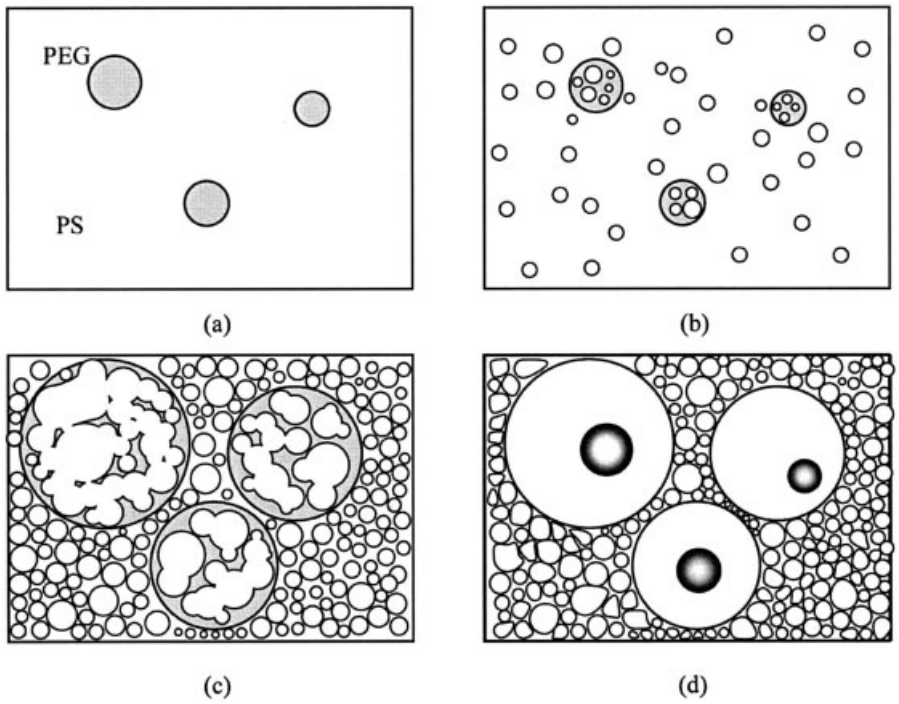

Figure 12 Schematic diagram of the formation mechanism of the bimodal cellular structure: (a) initial state, (b) bubble nucleation and growth, (c) bubble coalescence, and (d) particle formation.

bubble growth rate. Higher solubility and higher diffusivity make the bubble growth rate faster. As illustrated in Figures 1 and 2, the solubility and diffusivity of CO_2 in PEG were both larger than those in PS. The mass transfer of CO_2 from the polymer to a bubble became faster in the PEG phase than in the PS phase, and this resulted in the difference of the bubble growth rates illustrated in Figure 11.

Our previous study also indicated that shear and elongational viscosities controlled the coalescence of bubbles.[16] As shown in Figure 3, both the storage and loss moduli of PEG were smaller than those of PS. This means that bubble coalescence occurred easily in the PEG phase. As we could observe at the visual observation experiments, the bubble coalescence occurred frequently after the number of bubble nucleation ceased and eventually became close to a two-phase (gas and polymer) separation.

A formation mechanism of the cellular structure observed in the PEG/PS blend foaming is summarized in Figure 12. Before the foaming, the island (PEG particles)–sea (PS) morphology was established because of the immiscibility of both polymers. The dispersibility of PEG in the PS matrix was changed by the weight fraction and could be controlled by mixing. When the PS/PEG blend polymer was foamed, because of the high solubility of CO_2 in PEG, bubble nucleation and growth occurred in the PEG phase followed by those in the PS phase at the initial stage of foaming. Because of the higher diffusivity of CO_2 in PEG, the bubbles originating in the PEG phase grew faster and become larger than the bubbles nucleated in the PS matrix. The lower viscosity easily led to the PEG bubbles coalescing and to a two-phase separation in the PEG phase. As the temperature decreased, the cell structure stabilized. PEG in the large cells formed a particle because of the wettability of PEG against PS. These phenomena created a bimodal cell structure, in which the larger cell embraced a PEG particle.

At this point, there is no clear explanation for the experimental results that the existence of PEG reduced the cell size in the PS phase. However, because dissolved CO_2 reduces the viscosity of a polymer,[17–25] we can speculate about the reason as follows: larger cells originating in the PEG phase consume CO_2 faster and take up the CO_2 dissolved in the PS phase faster. The average concentration of CO_2 in the PS phase decreases faster, and the plasticization effect induced by CO_2 disappears faster at 110°C. As a result, the viscosity of the PS matrix suddenly increases and suppresses the bubble growth in the PS phase.

CONCLUSIONS

PEG/PS blends were physically foamed at 110°C and 10 MPa with CO_2. The foam showed a unique cellular structure in which large cells embraced a PEG particle and small cells existed around large cells. The mechanism of creating such a cell structure could be explained by the morphology of the blends, the solubil-

ity and diffusivity of CO_2 in each polymer, and the viscosity. This study might lead to the development of an efficient nucleating agent of polymer foaming. The number of large cells embracing a PEG particle was not large. However, because the dispersibility of large cells in a polymer foam strongly depends on the initial morphology, an enhancement of the mixing ability to homogeneously disperse PEG in a blend can create a fine bimodal cell structure and eventually create an open cell structure at will.

References

1. Dutta, A.; Cakmak, M. Rubber Chem Technol 1992, 65, 778.
2. Dutta, A.; Cakmak, M. Rubber Chem Technol 1992, 65, 932.
3. Yamaguchi, M.; Suzuki, K. J Polym Sci Part B: Polym Phys 2001, 39, 2159.
4. Doroudiani, S.; Park, C. B.; Kortschot, M. T. Polym Eng Sci 1998, 38, 1205.
5. Rachtanapun, P.; Selke, S. E. M.; Matuana, L. M. J Appl Polym Sci 2003, 88, 2842.
6. Lee, M. H.; Tzoganakis, C.; Park, C. B. Polym Eng Sci 1998, 38, 1112.
7. Siripurapu, S.; Gay, Y. J.; Royer, J. R.; DeSimone, J. M.; Spontak, R. J.; Khan, S. A. Polymer 2002, 43, 5511.
8. Krause, B.; Diekmann, K.; van der Vegt, N. F. A.; Wessling, M. Macromolecules 2002, 35, 1738.
9. Areerat, S.; Hayata, Y.; Katsumoto, R.; Kegasawa, T.; Egami, H.; Ohshima, M. J Appl Polym Sci 2002, 86, 282.
10. Sanchez, I. C.; Lacombe, R. H. Macromolecules 1976, 11, 1145.
11. Sanchez, I. C.; Lacombe, R. H. J Phys Chem 1976, 80, 2352.
12. Zoller, P.; Walsh, D. J. Standard Pressure–Volume–Temperature Data for Polymers; Technomic: Lancaster, PA, 1995.
13. Taki, K.; Yanagimoto, T.; Funami, E.; Okamoto, M.; Ohshima, M. Polym Eng Sci 2004, 44, 1004.
14. Taki, K.; Nakayama, T.; Yatsuzuka, T.; Ohshima, M. J Cell Plast 2003, 39, 155.
15. Kumar, V.; Suh, N. P. Polym Eng Sci 1990, 30, 1323.
16. Taki, K.; Tabata, K.; Kihara, S.; Ohshima, M. Proceedings of Foams; Society of Plastic Eng., TM&F Division: Wilmington, DE, 2004.
17. Kwag, C.; Manke, C. W.; Gulari, E. J Polym Sci Part B: Polym Phys 1999, 37, 2771.
18. Royer, J. R.; Gay, Y. J.; Desimone, J. M.; Khan, S. A. J Polym Sci Part B: Polym Phys 2000, 38, 3168.
19. Lee, M.; Tzoganakis, C.; Park, C. B. Adv Polym Technol 2000, 19, 300.
20. Elkovitch, M. D.; Lee, L. J.; Tomasko, D. L. Polym Eng Sci 2000, 40, 1850.
21. Elkovitch, M. D.; Lee, L. J.; Tomasko, D. L. Polym Eng Sci 2001, 41, 2108.
22. Kwag, C.; Manke, C. W.; Gulari, E. Ind Eng Chem Res 2001, 40, 3048.
23. Utracki, L. A.; Simha, R. J Polym Sci Part B: Polym Phys 2001, 39, 342.
24. Han, X. M.; Koelling, K. W.; Tomasko, D. L.; Lee, L. J. Polym Eng Sci 2002, 42, 2094.
25. Xue, A. L.; Tzoganakis, C. J Polym Eng 2003, 23, 1.